8th International Symposium on Magnetic Bearing
August 26-28, 2002, Mito, Japan

IMPROVED POSITION CONTROL OF A MAGNETIC GUIDE USING ACCELERATION MEASUREMENT AND A LASER POSITION REFERENCE

Martin Ruskowski
Institut für Mechanik, Universität Hannover, D-30167 Hannover, Germany
ruskowski@ifm.uni-hannover.de
Karl Popp
popp@ifm.uni-hannover.de

ABSTRACT

Active magnetic guides (AMG) qualify as an alternative guiding principle for many machine tool applications. As active magnetic bearings (AMB) in rotational applications they avoid friction forces and wear. Tests on a prototype AMG showed that an adequate dynamic stiffness for a machine tool axis can be achieved. Still this comes along with a high sensor noise susceptibility as the determination of the velocity requires high observer gains. A measurement of other states next to the displacement can improve the dynamic stiffness of the control significantly. It will be shown that measuring the absolute acceleration vector can improve the dynamic stiffness nearly by a factor of three without modifying the controller gain.

Often the precision of mechanical rails as a reference for the position control is insufficient. Here, an absolute position reference can be used to increase the positioning accuracy perpendicular to the feed direction. Since optical laser based sensors are applicable to this problem, a five-degree-of-freedom sensor has been built for the prototype guide and used as an absolute position reference. Measurements show an accuracy of about 5 µm can be achieved over the full stroke.

INTRODUCTION

Possible applications for AMGs include High Speed Cutting (HSC) machine axes or long-stroke, high speed machines as used e. g. in the wood processing industry. AMGs have extreme advantages in clean rooms as in harsh environments, since no lubrication and no sealing of the active parts is required.

In a joint research project at the University of Hannover, a new generation of High Speed Cutting machines aiming at accelerations of 5 g is under development. Our project part deals with the integration of an AMG as an axis for a new type HSC machine.

Experimental setup

For an examination of the achievable control dynamics that provides the mechanical stiffness, a prototype guide (cp. Fig. 1) had been built [1,2]. It consists of an aluminum frame with a steel reinforcement and has a mass of 45 kg. The additional payload can be up to 100 kg. The frame is guided by six pairs of electromagnets in differential arrangement. Six eddy current displacement sensors are used to measure the position relative to the rails.

The control is realized on a 366 MHz PowerPC VME process computer using the hard real-time operating system RTOS-UH from Hannover University [3]. The system is capable to generate flexible sample rates of up to 20 kHz while being used as a general purpose computer. The controller is written in the high level real-time language PEARL allowing for efficient multitasking real-time programming.

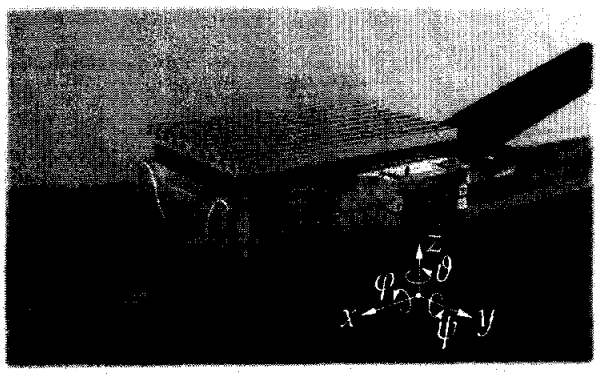

FIGURE 1: The active magnetic guide (AMG).

CONTROL LAYOUT

The control strategy used for the AMG is a decoupled cascade control (DCC) and has been previously published [1-2]. It can be easily adapted to any configuration of AMGs. It is designed to control the five degrees of freedom (DOF) excluding the feed direction x.

Decoupled cascade control (DCC)

The basic idea of the controller is to decouple the five controlled degrees of freedom via an inverse model of the (constant) couplings in the plant (cp. Fig. 2). This is performed via the mass matrix M and the (constant) Jacobian $J = \partial x / \partial q$, where the magnet displacements from the nominal air gap are given by the (6x1) vector $x = s - s_0$ and the guide displacement is denoted in generalized coordinates by the (5x1) vector

$$q = [y\ z\ \varphi\ \psi\ \vartheta]^T \tag{1}$$

(cp. Fig. 1) for a fixed reference point B in the geometrical center of the guide. The AMG is overactuated since it has more actuators than degrees of freedom. Thus, for the calculation of the necessary magnet forces F it is not possible to invert J directly since it is non-square. Instead, the transposed pseudo-inverse $(J^T)_p^{-1} = J(J^T J)^{-1}$ is used which resolves the overdetermination is the least squares sense. The magnet forces are calculated from the desired acceleration vector $\ddot{q}_d$ as

$$F_d = J(J^T J)^{-1} M \ddot{q}_d. \tag{2}$$

The position of the guide relative to the rails is measured using six eddy current displacement sensors. The generalized deflection q is calculated from the sensor vector x_s using the pseudo-inverse $(J_s)_p^{-1} = (J_s^T J_s)^{-1} J_s^T$ of the sensor Jacobian J_s.

Actuator model

The current necessary to achieve the desired force is calculated using an inverse model of the magnet characteristics. Usually a linear relation

$$F = k_i i + k_s x \tag{3}$$

with gain k_i and negative bearing stiffness k_s is used. Then,

$$i_d = \frac{F_d - k_s x}{k_i} \tag{4}$$

gives the desired current i_d from the desired force F_d. This linear formulation is well suited for differential magnet arrangements as with the prototype, where the nonlinearities of the magnets compensate each other.

For magnet arrangements not based on differential magnets a linear model is no longer sufficient. For this purpose a nonlinear model has been developed [4]. This model provides the currents from the desired force F_d and the air gap $s = s_0 + x$ via a nonlinear function or a two dimensional table lookup.

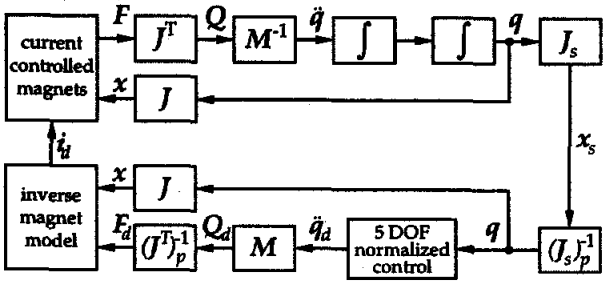

FIGURE 2: Layout of the DCC loop.

The magnets are sourced by switched power amplifiers with integrated analogue current control. This concept has proven to be very robust. Current control is essential since the DCC needs a simple actuator model. The power amplifiers used for the prototype have a maximum current of 4 A at a voltage level of 130 V. The control bandwidth is > 600 Hz. Eddy current losses in the massive iron rails are compensated using high-pass filters [4].

Normalized Control

The control itself is designed in a normalized domain for the generalized coordinates q, calculating the desired generalized acceleration $\ddot{q}_d$ from the displacement vector q, thus the reference position is given as $q_d = 0$. For an optimal suppression of sensor noise, the control is realized as five independent discrete-time PID-equivalent controllers with KALMAN-filters for the observation of the velocities. Due to the normalization the plant model for a single degree of freedom $i \in \{y, z, \varphi, \psi, \vartheta\}$ is given by the extended state space description for the state vector $y_i = [\int q_i dt\ q_i\ \dot{q}_i]^T$

$$y_{i,k+1} = A y_{i,k} + B u_i \tag{5}$$

$$q_i = C y_{i,k} \tag{6}$$

where

$$A = \begin{bmatrix} 1 & T & T^2/2 \\ 0 & 1 & T \\ 0 & 0 & 1 \end{bmatrix},\ B = \begin{bmatrix} T^3/6 \\ T^2/2 \\ T \end{bmatrix},\ C = [0\,1\,0].$$

The control feedback is given by the matrix F according to

$$\ddot{q}_{i,d} = F y_i. \tag{7}$$

To achieve maximum damping, F is chosen as

$$F = \begin{bmatrix} s_c^3 & -3s_c^2 & 3s_c \end{bmatrix}, \tag{8}$$

resulting in a nominal triple pole of the closed loop system at $s = s_c$, thus the nominal damping ratio is $D = 1$.

KALMAN-filter based state observer

For the normalized control – as with all magnetic bearing control – the determination of the air gap velocity is crucial to achieve a high damping ratio. For this purpose, five parallel KALMAN-filters are implemented as optimal state observers (cp. Fig. 3). They are only designed for the reduced observer state vectors $\hat{y}_i = [\,\hat{q}_i \;\; \hat{\dot{q}}_i\,]^T$, since the integral parts need not to be observed.

The KALMAN-filter design [5] is based on the process noise covariance matrix Q and the measurement noise covariance matrix R. It uses a gain matrix $K_{i,k}$ varying with time kT as observer feedback. The filter is updated every time step k according to the time update equations

$$\hat{y}^-_{i,k} = \tilde{A}\hat{y}_{i,k-1} + \tilde{B}u_{i,k} \tag{9}$$

$$P^-_{i,k} = \tilde{A}P_{i,k-1}\tilde{A}^T + Q \tag{10}$$

and the measurement update equations

$$K_{i,k} = P^-_{i,k}\tilde{C}^T(\tilde{C}P^-_{i,k}\tilde{C}^T + R)^{-1} \tag{11}$$

$$\hat{y}_{i,k} = \hat{y}^-_{i,k} + K_{i,k}(q_{i,d} - \tilde{C}\hat{y}^-_{i,k}) \tag{12}$$

$$P_{i,k} = (I - K_{i,k}\tilde{C})P^-_{i,k} \tag{13}$$

with the error covariance matrix P.

To achieve a high dynamic stiffness, the process noise covariance matrix Q for the KALMAN-filter has to be chosen quite high thereby degrading the advantages of the observer layout. This is why in many AMB applications still numerical derivation is used instead of state observation.

Experiments show the maximum of the dynamic compliance as a performance criterion for the control cannot be pushed beyond a point where the sensor noise is amplified so high that spill over effects occur. Thus, the presented control based on the air gap signal only is limited in its performance.

Acceleration measurement

For the steady state case, a smart disturbance compensation can achieve a significant improvement [8]. For transient disturbances a better velocity determination is required using velocity or acceleration sensors. Simulations show the effect of acceleration measurement to be of greater effect than that of the velocity, as the integration of the acceleration signal over time low-pass filters the sensor noise. Further, acceleration sensors are standard laboratory equipment and available at moderate prices in industry-compatible housings whereas velocity sensors are not widely used.

Therefore, the prototype guide has been equipped with five-degree-of-freedom acceleration measurement, cp. Fig. 4. Two biaxial and one single axis

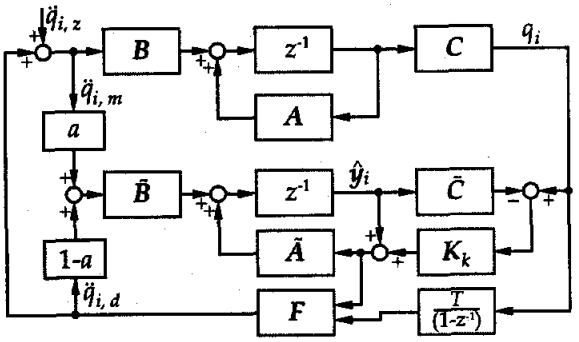

FIGURE 3: Layout of one KALMAN-filter based state controller with acceleration measurement.

sensor are combined to measure the full five DOF acceleration vector. The transformation from the acceleration sensor coordinates to the generalized coordinates is performed using the inverse of the corresponding Jacobian J_a. If more than five accelerations are measured, again the pseudo-inverse of J_a should be used.

The measured generalized acceleration vector $\ddot{q}_m$ is fed as an additional input to the five KALMAN-filters, cp. Fig. 3. It is blended by a factor a, $0 \leqslant a \leqslant 1$ with the desired acceleration signal $\ddot{q}_d$, the output signal of the normalized control. For $a = 0$ only $\ddot{q}_d$ is used whereas $a = 1$ means only $\ddot{q}_m$ is taken as observer input, thus, a disturbance $\ddot{q}_z$ directly influences the observer. A blending factor of about $a = 0.8$ has shown to be a good choice since the acceleration signal is also noisy.

Results

To evaluate the profit gained by the acceleration measurement, frequency responses due to an external force have been measured for varying parameters a. The force has been applied using an electrodynamic shaker in vertical z-direction directly above the reference point B in the symmetrical cen-

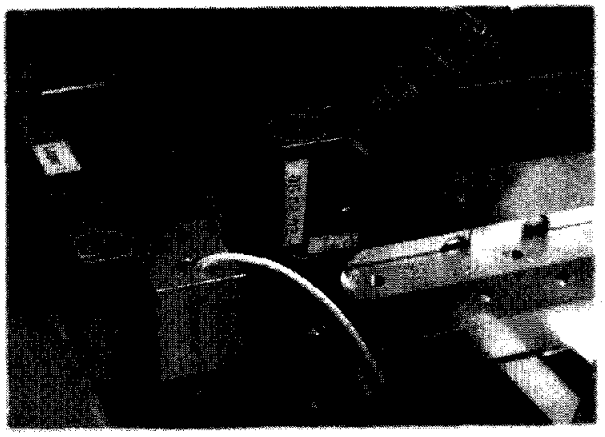

FIGURE 4: Closeup of magnet, displacement sensor and biaxial acceleration sensor.

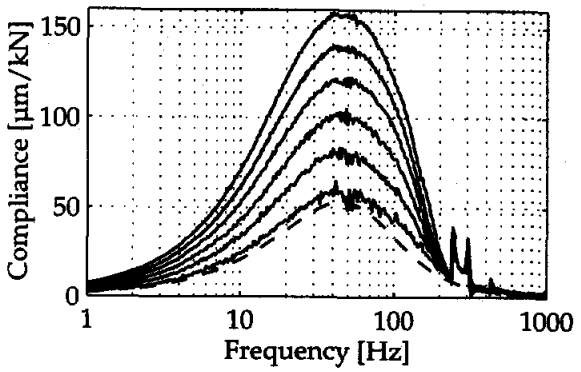

FIGURE 5: Measured frequency response $G_{zz}(f)$, $a = 0.0/0.2/0.4/0.6/0.8/1.0$ (solid, from top to bottom) and theoretical limit (dashed).

ter of the guide. An external exciter is necessary since the levitation magnets have a limited bandwidth due to eddy current losses [4] and therefore cannot be used as excitation source.

The force of the exciter has been measured by a force sensor and controlled to a fixed amplitude of 50 N, the exciter limit. The DCC was fixed to a sample time of $T = 100\,\mu s$ and triple poles at $s_c = -400\,s^{-1}$. The noise covariances were chosen to $R = 10^{-12}$ and $Q = \mathrm{diag}[\,T^2\ T^4/4]$.

Fig. 5 shows the frequency response of the vertical z-direction to the external force. The blending factor a is varied from 0 to 1 in steps of 0.2. At $a = 0$ (top solid line), the maximum of the compliance is $G_{zz,max} = 160\,\mu m/kN$ at $f = 45\,Hz$. For $f \to 0$ and $f \to \infty$, G_{zz} approaches zero due to the integral control and the inertial mass, respectively. With increasing a the maximum of the compliance is reduced while the resonance frequency remains the same. This behavior is different from higher controller gains, where the resonance frequency increases with decreasing $G_{zz,max}$. At $a = 1$ (bottom solid line) the measured compliance almost coincides with the theoretical limit (dashed) where the velocity is known exactly. The maximum is at $G_{zz,max} = 55\,\mu m/kN$. Thus, with acceleration measurement the control is almost three times as stiff as without at the same controller dynamics.

Another benefit of the acceleration measurement lies in the reduction of cross couplings between the degrees of freedom due to modelling errors. As an example, Fig. 6 shows the pitch (ψ) motion frequency response $G_{z\psi}$ to the same vertical (z) force excitation. For low values of a a rather large response is obvious. This results from neglecting of the power chain mass (cp. Fig. 1) in the model. For larger values of a the coupling is removed almost completely. Thus, not only the stiffness is increased but also the control allows for more modelling errors at a higher control quality.

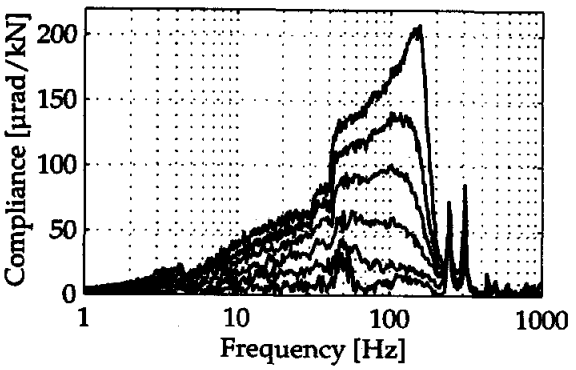

FIGURE 6: Measured frequency cross response $G_{z\psi}(f)$, $a = 0.0/0.2/0.4/0.6/0.8/1.0$ (from top to bottom).

The peaks at 245 and 305 Hz in Fig. 5 and 6 are artifacts due to resonances of the exciter's steel rack, thus showing the AMG is almost as stiff as a solid steel construction.

Sensor resolution considerations

Although the acceleration sensors used for the control have a nominal noise level of $1\,mm/s^2$, the measured acceleration signal show a rather high noise level of about $1\,m/s^2$ resulting from electromagnetic disturbances like the switched power amplifiers and other sources.

For the application as KALMAN-filter input this high noise level shows to be of low significance. The numerical integration of the acceleration signal at a sample rate of 10 kHz suppresses most of the noise. Thus, low cost 10 bit sensors from automotive applications instead of high-end 16 bit laboratory sensors should be sufficient, as the maximum required measurement range is of the order of $50\,m/s^2$.

ABSOLUTE LASER BEAM POSITION SENSOR

Usually, AMGs take the guiding rails as a position reference. This leads to positioning errors due to the mechanical unevenness of the guiding rails' surface. This is especially true for guides with long feed ranges. Here, a precise absolute position reference could increase the positioning accuracy in the degrees of freedom perpendicular to the feed direction while the mechanical construction may be less precise and therefore cheaper.

Optical laser beam sensors (LBS) fulfill these demands. They can be expanded to multi-degree-of-freedom sensors. A five-degree-of-freedom laser beam sensor has been constructed and applied to the prototype AMG. All parts of the sensor including the mechanics, amplifiers and analog-to-digital converters have been constructed at our lab specifically to the needs.

Sensor principle

Position sensing detectors (PSDs, cp. Fig. 7) in combination with laser beams are well known and widely used in linear and angular position measurement, e. g. in commercial triangulation sensors. They consist of a planar photo diode with two (linear PSD) or four electrodes (planar PSD). A laser spot hitting the PSD surface results in a photo current I which splits to the electrodes according to the position of the center of the spot on the PSD.

The position of the laser spot on the linear PSD is given by

$$\xi = \frac{\ell}{2}\frac{I_A - I_B}{I_A + I_B} \tag{14}$$

where ℓ is the active length and $\xi = 0$ characterizes the center of the PSD. The absolute value of the photo currents I_A and I_B depends on the light intensity of the laser spot, whereas the position is independent of the intensity and very linear (about 0.5% of full scale range, [7]). For the planar PSD this relation is valid independently for each of the two coordinates η and ζ, respectively.

A one-degree-of-freedom laser beam sensor based on a linear PSD had been built and tested on a different test stand in our lab [8]. It has a lateral resolution of less then 10 µm at a distance of 2.5 m and a lateral measurement range of ±5 mm.

For a multi-DOF-sensor several PSDs can be combined to measure linear and angular displacements. Several arrangements are possible for this purpose. For an AMG a five-DOF-sensor is required, since this is the number of controlled degrees of freedom. As it is desirable to use identical sensors, an arrangement of three planar sensors is a good choice. The redundancy further reduces errors.

Sensor arrangement

Fig. 8 shows the chosen configuration for the realized sensor. Beam splitter 2 and mirror 3 are slanted with respect to the (x,y)-plane, thus enabling the laser beam to reach PSD 3 without passing splitter 2 again. Thus, optically PSD 3 is positioned in line with PSD 2 and the laser beam. The two laser beams necessary can be separated from a single laser diode using a beam splitter and a mirror. Mirror 1 is only used to minimize the space needed in the transmitter.

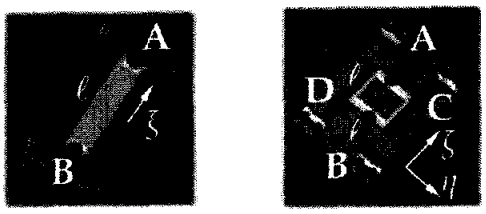

FIGURE 7: Linear (left) and planar PSD (right) [7].

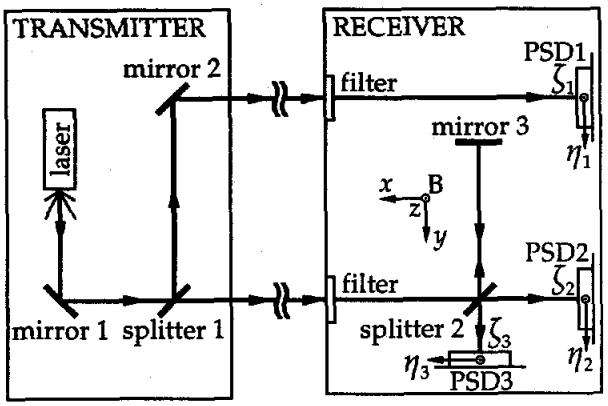

FIGURE 8: Arrangement of laser transmitter and receiver with the PSDs.

PSD i measures a deflection vector $x_{\ell,i} = [\,\eta_i\ \zeta_i\,]^T$ in the (y,z)-plane, respectively. The PSD deflections are linked to the generalized coordinates q via

$$x_{\ell,i} = J_{\ell,i}\, q. \tag{15}$$

Combining the three PSDs leads to

$$x_\ell = J_\ell\, q. \tag{16}$$

As already for the position and acceleration sensors, again the pseudo-inverse of J_ℓ can be used to transform the PSD deflections to the generalized coordinates,

$$q_\ell = (J_\ell^T J_\ell)^{-1} J_\ell^T\, x_\ell. \tag{17}$$

Control layout

The laser beam reference is applied as an outer control loop to the DCC (cp. Fig. 9). It can be implemented with a lower sampling rate as a five-degree-of-freedom PI-controller tracking the reference position q_d of the inner control loop to match the offset measured by the laser beam sensor.

Hardware realization

The LBS is designed with the transmitter fixed to the rail support and the receiver mounted within the guide itself. Optical filters at the inlet of the otherwise completely closed receiver box reject daylight influences almost completely.

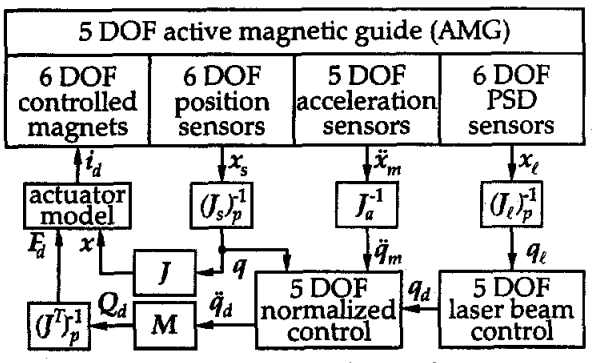

FIGURE 9: Control loop with laser beam sensor.

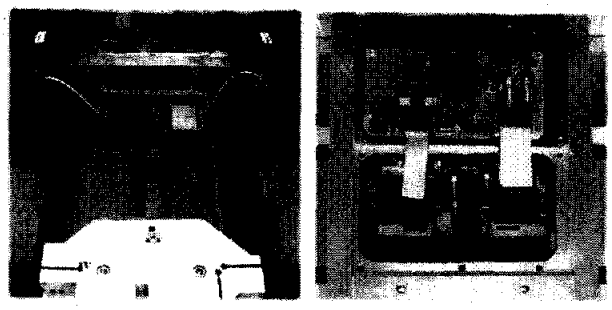

FIGURE 10: Transmitter, laser beams and AMG (left). Receiver (cover opened) with PSD sensors, precision amplifiers and A/D conversion hardware (right).

Careful consideration has been given to the measurement of the PSD signals. Since the photocurrents of the PSDs are smaller than 100 µA, an immediate on-the-spot precision amplification is crucial. To further improve the performance, not only the amplification but also the 16 bit analog-to-digital conversion is performed within the shielded sensor housing thus minimizing electromagnetic susceptibility problems.

The link to the VME host computer is made up through a proprietary serial RS-422 connection at a data rate of 4 Mbit/s. Thus, up to 16 channels can be converted at a maximum sample rate of 10 kSamples/s of which the laser beam data acquisition uses only 12 channels (four channels per PSD) at the 1 kHz sample rate of the tracking controller.

The A/D-converters used are fast audio converters with a high linearity and low distortion. The sensor is completely powered from the VME system and the design incorporates a separated supply potential from the VME-System using DC/DC converters and optocouplers. The effective noise of the converters is below 2 bit. Due to the high quality of the conversion hardware, the same converters have been implemented for the position and acceleration sensors using the full 10 kHz sample rate.

Results

The implementation of the laser beam sensor shows it to be a possible absolute position reference for the DCC. The noise level of the PSDs and the positioning accuracy lies below 5 µm.

Still the PSD position noise is an order of magnitude larger than that of the eddy current sensors, so they cannot be replaced. This agrees with the necessity of the DCC to know the true air gap of the magnets for a nonlinear inverse magnet model. As the laser beam only measures the absolute displacement it cannot provide any information on the relative displacement between guide and guiding rails.

Two minor drawbacks have to be mentioned. The laser beam sensor is only as precise as its calibration, as the two laser beams have to be exactly in parallel with respect to each other and the desired axis. Furthermore, the fluctuation of the beam due to thermal effects in the air is another point. Thus, covering the beams might be necessary.

CONCLUSIONS

The paper has shown that the position control of an active magnetic guide (AMG) can be improved significantly using enhanced sensor hardware. The measurement of the acceleration vector improves the dynamic stiffness by a factor of three with the same controller gain. In combination with a KALMAN-filter as optimal state observer the velocity can be estimated truly so the performance reaches almost the theoretical limit.

For long-stroke AMGs an absolute position reference can increase the positioning accuracy to within several µm perpendicular to the feed direction. This qualifies AMGs for many new precision machining applications.

REFERENCES

[1] Tieste, K.-D., *Mehrgrößenregelung und Parameteridentifikation einer Linearmagnetführung*, PhD Thesis, VDI-Fortschrittsberichte Reihe 8, Band 656, Düsseldorf 1997.

[2] Ruskowski, M. and Popp, K., *A Contactless Axis for High Speed Cutting Machines*, Proc. 4th Int. Conference on Motion and Vibration Control MOVIC, Vol. 3, pp. 1095-1099, Zürich 1998.

[3] RTOS-UH/PEARL Real Time Operating System, `http://www.rtos-uh.de`

[4] Ruskowski, M. and Popp, K., *Nonlinear Modeling of a Magnetically Guided Machine Tool Axis*, 7th International Symposium on Magnetic Bearings ISMB-7, pp. 413-418, Zürich 2000.

[5] Welch, G. and Bishop, G., *An Introduction to the Kalman Filter*, `http://www.cs.unc.edu/~welch/media/pdf/kalman_intro.pdf`

[6] Ruskowski, M., Reicke, L. and Popp, K., *Enhanced Steady State Stiffness for a Magnetic Guide using Smart Disturbance Compensation*, 6th Int. Conference on Motion and Vibration Control MOVIC, Saitama 2002.

[7] Laser2000, *Messtechnik für Laser und Optoelektronik*, `http://www.laser2000.de/pdf/optischemesstechnik/positio1.pdf`

[8] Reckmann, H., *Aktive Schwingungsreduktion an einem elastischen Fahrweg unter bewegter Masse*, PhD Thesis (in print).